VTT PUBLICATIONS 703

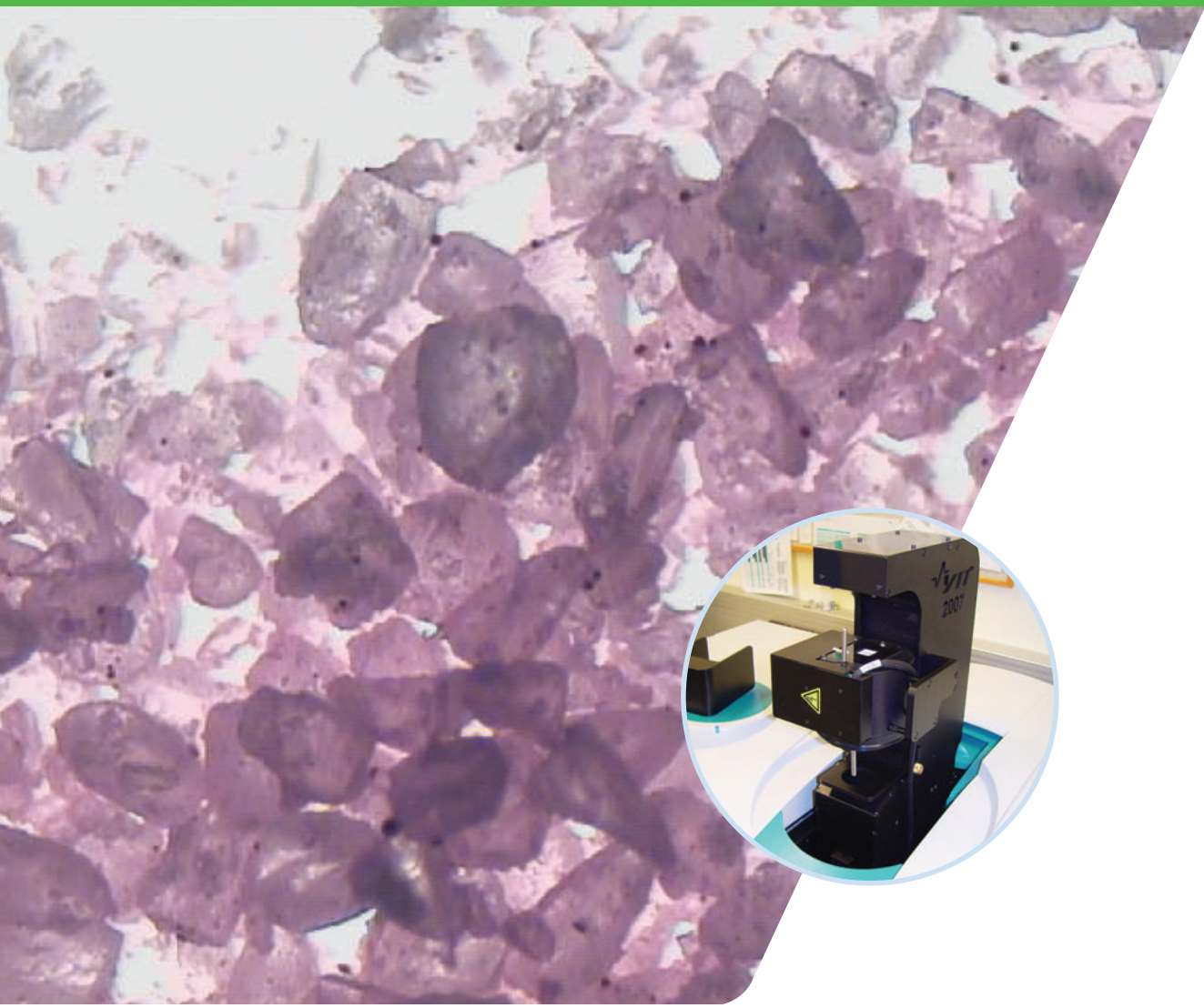

Lauri Kurki & Ralf Marbach

Radiative transfer studies and Next-Generation NIR probe prototype

VTT PUBLICATIONS 703

Radiative transfer studies and Next-Generation NIR probe prototype

Lauri Kurki & Ralf Marbach

ISBN 978-951-38-7137-6 (soft back ed.)
ISSN 1235-0621 (soft back ed.)

ISBN 978-951-38-7333-2 (URL: http://www.vtt.fi/publications/index.jsp)
ISSN 1455-0849 (URL: http://www.vtt.fi/publications/index.jsp)

JULKAISIJA – UTGIVARE – PUBLISHER

VTT, Vuorimiehentie 5, PL 1000, 02044 VTT
puh. vaihde 020 722 111, faksi 020 722 7001

VTT, Bergsmansvägen 5, PB 1000, 02044 VTT
tel. växel 020 722 111, fax 020 722 7001

VTT Technical Research Centre of Finland, Vuorimiehentie 5, P.O. Box 1000, FI-02044 VTT, Finland
phone internat. +358 20 722 111, fax + 358 20 7001

Layout by Tarja Haapalainen

Edita Prima Oy, Helsinki 2009

Lauri Kurki & Ralf Marbach. Radiative transfer studies and Next-Generation NIR probe prototype. Espoo 2009. VTT Publications 703. 43 p.

Keywords NIR, spectroscopy, Monte Carlo, radiative transfer, diffusion, SDR, diffuse reflectance, diffuse transmittance, structured illumination

Abstract

As a part of the PAT-KIVA project, this report summarizes the results of the work packages (WP's) 1.1 and 1.4. The WP1.4 consisted of laboratory studies to measure the absorption and scattering properties of several pharmaceutical powders. It also included the designing and building of the spectrometer accessories to make the measurements possible. The WP1.4 was needed to support of the WP1.1, where a wireless online probe of powder blend homogeneity was to be built. The idea was to be able to separate the chemical concentrations from the physical determinants of the powder blends by spatially resolved diffuse reflectance spectroscopy (SDR). The chemical concentrations were assumed, according to previous studies by others, to be faithfully represented in the calculated absorption coefficient. On the other hand, the physical properties like particle size distribution were assumed to be separated into the scattering coefficient and anisotropy factor. However, the studies indicated, that with the growth of particle size, these assumptions do not hold to any reasonable degree. Therefore it was decided not to design the online probe, but a laboratory research probe employing the SDR principle and being as versatile as possible regarding the wavelength range and illumination features. The design of the laboratory probe was nearly completed, but due to various reasons, it could not be built within the PAT-KIVA project. The main results of the WP1.4 were the building of spectrometer accessories and the measured optical properties of various powders. The main results of the WP1.1 were the preliminary comparison of SDR measurements to the "reference" measurements done in WP1.4, and the near completion of the very challenging design task of the laboratory SDR probe. Another main result connected with both work packages was the development of simulation software to solve the inverse problem of calculating samples' optical properties from spectroscopic measurements.

Preface

This work was carried out in VTT Technical Research Centre of Finland in the Knowledge Center of Optical Instruments during years 2007 and 2008. The study was financed by TEKES, Finnish Funding Acendy for Technology and Innovation, and by the large industrial group (GlaxoSmithKline, Orion, Bayer-Schering, Metso Automation, Specim, KSV Instruments, Genecor International, Exens Instruments and Unilever) supporting the collaboration project called "PAT-KIVA", PAT to National Success.

PAT-KIVA project comprised seven collaborating parties: at University of Helsinki, Departments of Pharmaceutical Technology and Physical Sciences; at University of Kuopio, Departments of Pharmaceutics and Physics; Lappeenranta University of Technology, Laboratory of Separation Technology, and at VTT, Optical Instruments and Process Chemistry Centres.

The aim of the present public consortium project is to build up a new PAT platform in Finland, which combines knowledge of public basic research on PAT in different fields of expertise with development of process instrumentation technology. In the present platform, current national public research on PAT meets the Finnish industry that could directly exploit the results to their manufacturing processes and applications.

In this work, the theoretical models, the powder measurements and the three prototype designs have been done in VTT. The experimental design of powder measurements and the prototype specifications have been done in collaboration with VTT and University of Kuopio, Department of Pharmaceutical Sciences. All research and industrial parties are gratefully acknowledged.

Oulu 13.1.2009

Lauri Kurki and Ralf Marbach

Contents

1. Introduction

Many PAT methods are based on UV, VIS, or NIR spectroscopy and many of the samples relevant for pharmaceutical applications are turbid, i.e. optically scattering. The measured spectrum is therefore dependent on *two* spectral properties, viz. the absorption and the scatter coefficient of the sample. The dependence on the absorption coefficient is usually desired, of course, but the dependence on the scatter coefficient is often an undesired flaw.

One PAT example is NIR spectroscopy of blend uniformity of a powder mixture. Here, the instrument "looks" into the blender through a view window located in the container wall, and measures a diffuse-reflection spectrum. The purpose of the measurement is end-point detection, because rotating the blender more often than necessary can cause milling effects and a corresponding "de-mixing" as the particle size distribution changes. Depending on various factors, e.g., particle size variations in the incoming raw materials; the packing density of the powder lying on the window will change, which in turn will change the scatter coefficient, which in turn will change the effective optical pathlength with which the powder sample is probed in diffuse reflection. As a result, batch-to-batch accuracy is challenging and even within a single batch, calibration of analyte concentration profiles is challenging unless the optical pathlength happens to stay reasonably constant throughout the whole duration of the batch.

Many “successful” studies of NIR blend uniformity have been presented, but “success” generally meant that the endpoint was detected in an indirect way, viz. by just comparing how similar the spectra were to each other but not by relating the spectra to the actual component concentrations in the mixture. For pharmaceutical applications, where the whole focus is on science-based decision making, this situation is undesirable. Validation of any indirect (statistical) method is much more laborious and expensive compared to methods where the underlying physical principles are clear.

The struggle to eliminate, or at least stabilize, the influence of the scatter coefficient is probably as old as is spectroscopy itself (Kubelka-Munk theory). In recent years, the most interest in the subject has come from the biophotonics community. Consequently, in the NIR at least, human skin has come into use as a well-characterized optical “standard”.

The overall strategy chosen by VTT OIC in this project has been to develop an NIR instrument that can (a) perform a diffuse reflection measurement similar in geometry to today’s instruments (i.e., one big spot of light on the sample for both illumination and pickup, approx. Ø25 mm) and can also (b) perform one or more “transmission” measurements on the same general sample area. Determination of the optimal measurement geometry suitable for pharmaceutical powders requires a significant amount of pre-study work, and was reflected in the task list of the project. Choice of sampling geometry is dependent on the optical properties of the sample, because the geometry must be selected so that the inversion process works reliably. Various tradeoffs are also considered. The optical properties of a number of different powder materials have been studied and the specifications for the prototype have been selected to be as broadly applicable as possible.

In all, the main goal in this project strategy has been to realize a new type of “front optics”, i.e. **Next-generation NIR probe prototype**, which, in principle, can be combined with any (non-imaging) spectrograph and which can measure two or three or more different geometries sequentially in time, but switching very fast, viz., on the order of tens of milliseconds.

2. Light propagation models in powder samples

This section is about the Monte Carlo (MC) light propagation code and associated inversion code developed further in the WP 1.1. The basic version was developed in an earlier project, but substantial refinements have been necessary and were implemented within WP 1.1. The section about the Next Generation NIR probe tells more about the practical advantages of Monte Carlo simulation as a part of spectroscopic measurement technology and limitations therein.

In short, the problem addressed by the toolbox is that of calculating the optical properties of a sample from two or more spectra measured with some given optical geometries. This task consists of implementing a *forward model*, and solving the *inversion* problem. A forward model is able to simulate the spectra when the optical properties are known. The inversion means finding the unknown optical properties of a sample, by the use of the measured spectra and the forward model. The MC simulation of light propagation is the forward model, and the inversion is done using the multivariable Newton iteration with Broyden method to update the Jacobian [Yaroslavsky et al. 1996].

The MC software package, or toolbox, consists of a DLL (Dynamically Loadable Library) and Matlab interface. The DLL, which is written in C language, is based on a public domain code MCML, and has been modified and for a large part rewritten to accommodate the demands of our measurements. The DLL calculates the forward model, i.e. MC simulation of light propagation in a layered sample with given optical properties. The Matlab interface handles the setting up of simulation geometries and inversion procedures. It has facilities for direct inverse Monte Carlo and several schemes for using pre-calculated MC simulation data for quick and stable inversion.

2.1 Radiative Transfer Model

There are a number of more and less realistic and respectively more or less computationally intensive ways to simulate the radiation field in random scattering samples. The models differ in the way how the medium is modelled and whether the electric field intensity or vector amplitude is used. In one end is the approach of using geometrical optics to propagate a ray through the material which is modelled as a statistical ensemble of collections of macroscopic particles [Green et al. 2000]. In the other end the material is taken as a homogeneous collection of microscopic scattering centres (of which more below). Here either the field intensity and polarization state, or the vector amplitude itself is considered.

For our purposes the model employed has to meet two main requirements. First, it must capture the material properties in as small set of parameters as possible. Second, it must be reasonably easily modifiable for all measurement geometries. The Radiative Transfer Equation (RTE) [Chandrasekhar 1960, Burger et al. 1997, Burger & Fricke 1998], especially in its Monte Carlo ray-tracing implementation [Yaroslavsky et al. 1996, Wang et al. 1995], meets these requirements best. It has been proven to be reasonably applicable to a large array of materials since its inception in the domain of astrophysics. RTE has both fast semi-analytical solutions for certain simple geometries [Rozé et al. 2001, Maheu et al. 1984] and general ray-tracing algorithm which is customarily implemented in optical design software like TracePro and Zemax. The diffusion equation can be derived as a limiting case of RTE [Fantini & Franceschini 2002, Jacques & Pogue 2008]. There is also a correspondence between the Kubelka-Munk theory and RTE, although only in certain limits.

In the radiative transfer model, a medium is considered as a continuous or piecewise-continuous distribution of scattering centers. These centers have both absorption and scattering cross sections σ_a, σ_s and therefore their number density $n(\mathbf{r})$ determines the local absorption and scattering coefficients $\mu_a = n\sigma_a$, $\mu_s = n\sigma_s$ of the medium. The unit of n is inverse volume (e.g. cm^{-3}), the unit of the cross sections is area (e.g. cm^2), and thus the unit of the coefficients is inverse length (e.g. cm^{-1}). On the other hand, sometimes the area density g/cm^2 of a sample is a better measure of the amount of material than thickness. In this case the "thickness" is given in units g/cm^2, and the coefficients in the units cm^2/g.

A scattering centre is furthermore characterized by the phase function $p(\cos\theta)$, which represents the probability distribution of the cosine of the scattering angle θ within the scattering plane. Namely, if $\mathbf{s}_1$ and $\mathbf{s}_2$ are the unit vectors of the directions of the incoming and scattered beam, respectively, then $\mathbf{s}_1 \cdot \mathbf{s}_2 = \cos\theta$. The absorption and scattering coefficients, along with the phase function and effective refractive index of the medium are the necessary material parameters in the radiative transfer model. In the following, we will be discussing only the steady-state, i.e. time-independent radiative transfer.

The radiation field is described only by its spectral radiance $L(\mathbf{r},\mathbf{s};\nu)$, which is a scalar quantity proportional to the time average of the square of the harmonic electric field amplitude at frequency ν. For the model to work, it is necessary to assume that there is no spatial correlation among the locations of the scattering centers, so that scattered field intensities are incoherently added. Otherwise one would need to deal with the relative phases and polarization to calculate interferences properly [Mishchenko et al. 2002]. If the polarization state of light is wanted, but the medium can still be assumed random, the radiance must be augmented with the three other components of the Stokes vector. Also, the scattering phase function must be augmented to a 4×4 matrix, called the Müller matrix [Bohren & Huffman 1998, Kim et al. 2001].

The RTE is an integro-differential equation that the radiance (generally the Stokes vector) must satisfy at each point $\mathbf{r}$ and into each direction $\mathbf{s}$. At each point, the field depends only on the local optical properties and the values of the field at the immediate neighborhood. The time-independent RTE for a medium with no sources is

$$\mathbf{s}\cdot\nabla L(\mathbf{r},\mathbf{s};\nu) = -\mu_t(\mathbf{r};\nu)L(\mathbf{r},\mathbf{s};\nu) + \mu_s(\mathbf{r};\nu)\oiint p(\mathbf{r},\mathbf{s}\cdot\mathbf{s}';\nu)L(\mathbf{r},\mathbf{s}';\nu)\mathrm{d}\Omega' , \qquad (2\text{-}1)$$

where the dependence of the optical properties on both the location and frequency of the field is explicitly indicated. The gradient is taken with respect to $\mathbf{r}$. The RTE and a sufficient amount of boundary conditions determine the radiance in the given physical situation. RTE can be converted into an integral equation and it is well known that those can be solved by suitable Monte Carlo methods [Metropolis & Ulam 1949]. We will not go here into the proof that the used MC algorithm is such a solution, but only take it for granted since it has been proven for the diffuse reflection and transmission

There are caveats to applying the RTE to particulate samples with large particle size. The largeness causes problems when illumination and measurement spot sizes are not at least about an order of magnitude larger than the average

particle diameter. In that case the medium is no longer random in the scale of the measurement geometry, and the apparent "optical properties" will change from one location to other.

The *hidden mass effect* [Burger & Fricke 1998] is observed when the absorption coefficient of the material of the particles is so large that a penetrating beam is significantly attenuated by absorption inside one particle. In this case, even when the particle is inside a powder and therefore illuminated almost diffusely, the insides of the particle can contribute less to the absorption of the powder than if the particle was broken to smaller pieces and then distributed evenly. In other words the surface of the large particle absorbs an appreciable amount of the incident radiation and because of this the inner parts of that particle receive only little power and thus have only a small effect to the overall measured spectrum. The hidden mass effect causes the absorption coefficient of the powder to be smaller than what would naively be expected at the strong absorption bands of the material. Still in other words, the problem arises when the optical thickness of a particle is no more much smaller than 1, i.e. the attenuation is nonlinear (follows the exponential Beer-Lambert law to some degree).

Another important effect causing problems in the radiative transfer simulations of powders is the neglect of surface reflections from the particles [Wendlandt & Hecht 1966]. Take the Fresnel formula for reflectance of a beam perpendicularly incident from air on a surface. Let the material, to which the surface belongs, have complex refractive index $n+ik$. Then

$$R_F = \frac{(n-1)^2 + k^2}{(n+1)^2 + k^2}. \tag{2-2}$$

Typically in NIR, $1.2 < n < 1.6$ and $0 < k < 0.2$. Note that $\mu_a = 4\pi k/\lambda_0$, where λ_0 is the vacuum wavelength. For pure water, $k(2930nm) \approx 0.3$, which makes $\mu_a(2930nm) \approx 13000cm^{-1}$, which is considered quite strong absorption. For typical powder materials in NIR, the absorption index k is much smaller. For instance, if $n = 1.5$, increasing k from 0 to 0.2 increases R_F from 4% to 4.6%. Because in particulate media the scattering is due to surface reflections, stronger absorbers will also increase scattering, roughly speaking. Also, diffuse reflection measurements where the regular reflection from the sample surface is blocked using linear polarizers in the illumination and pick-up, show considerable changes in the absorbance spectra compared to those measured without polarizers [Wendlandt & Hecht 1966]. Thus, the relative strengths of regularly and diffusely reflected part of the measured radiation vary as a function of wavelength.

2.2 Note on reference materials

The solution of the inverse problem requires that the measured intensity spectra are somehow converted to the absolute photon numbers for the comparison to the MC simulations. That is, the known and unknown optical and electronic losses of the probe must be cancelled out by the use of a known reference. In general the reference sample must be such that for given illumination and pick-up geometry the ratio of the collected power to the power incident on the sample is known. In the case of integrating-sphere measurements of total reflectance, it is customary to use a Spectralon (or equivalent optical Teflon) sample. For those the absolute reflectance, typically with a perpendicular illumination beam, is known. For a general measurement geometry there is no ready-made method of producing such references.

Our solution is to calculate the optical properties of a suitable reference material by the integrating-sphere method and *simulate* the absolute optical response of the sample in the given source- and pick-up geometry. For the best results, not only μ_a and μ_s' but also g must be known accurately, since g can affect greatly for example the simulation of collimated transmission of samples of moderate optical thicknesses. The optical Teflon makes a good general-purpose reference sample and we have been using it as such in our studies employing several different measurement geometries. We have estimated its optical properties in VIS-NIR range to a reasonable accuracy.

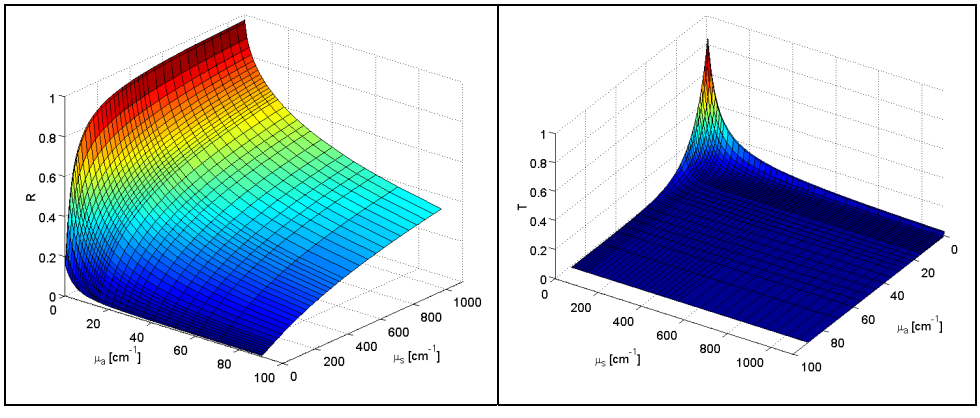

Figure 1. Simulated diffuse reflectance (left) and diffuse transmittance (right) of a 1 mm sample layer on top of quartz glass. Anisotropy g = 0.7.

2.3 Other models of diffuse reflectance

The radiative transfer model does not directly take into account the fact that a powder consists of macroscopic, irregular particles. The particulate nature of these samples has been considered in more physical models by Melamed et al. [Mandelis et al. 1990] and more recently in [Dahm & Dahm 2007]. Roughly these models treat the powder sample as a series of layers that consist of particles or their parts. The Melamed model is best suited for approximately monodisperse powders made of single material, whereas the Dahm model handles arbitrary mixtures. However, the models are not directly suitable for concentration measurements with arbitrary probe geometries.

3. Measurement equipment

We used the Varian Cary 5000 spectrophotometer equipped with two different integrating-sphere accessories as our “reference” system. The system supports the measurement of total diffuse reflection and transmission in the wavelength range 250–2500 nm. The maximum feasible absorbance for the system in transmission measurement is about 3 to 4.

One of the integrating-sphere accessories is the DRA-2500 sold by Varian Inc. (Figure 2). The sample is mounted vertically either on the reflectance or transmission port of the instrument. The integrating sphere unit has built-in detectors, a photomultiplier tube for UV-VIS (250–850 nm) and PbS detector for NIR (850–2500 nm).

Figure 2. DRA-2500 integrating-sphere accessory for Varian Cary 5000 spectrophotometer.

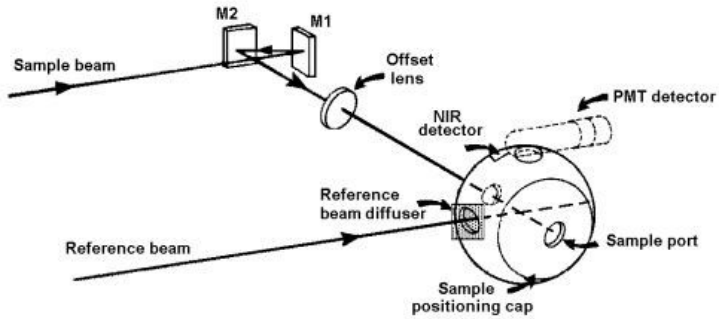

Figure 3. Optical design of DRA-2500 (by Varian Inc.)

For powder samples, it was seen as more appropriate to be able to mount the samples horizontally on top of a single glass slide. In the case of DRA-2500, the powder has to be poured between two glass slides in vertical position, which makes controlling of the sample density and size separation hard. Thus, another accessory was designed and built (Figure 4). The new accessory features an integrating sphere detached from a DRA-2500, so the detector electronics do not require changes. The optical design is based solely on mirrors to avoid chromatic aberration problems in the large wavelength range used.

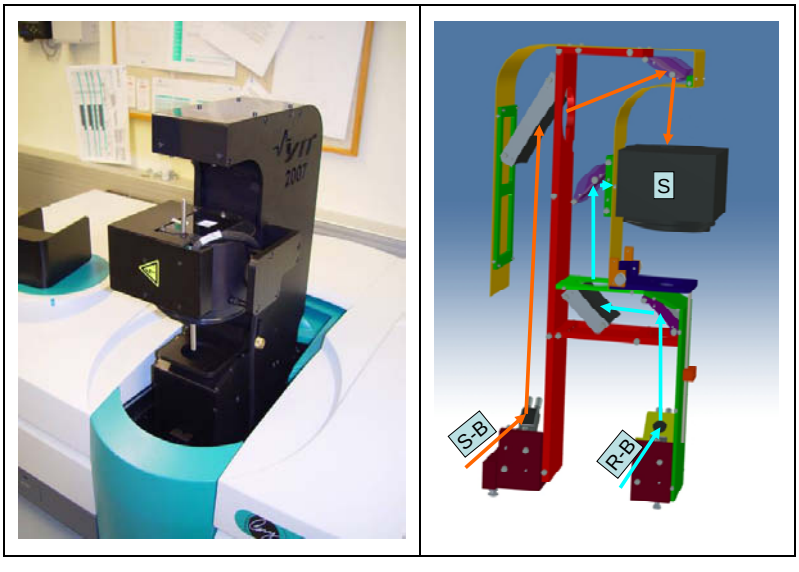

Figure 4. New integrating-sphere accessory by VTT, installed in Varian Cary 5000. **Left**: Installed to the spectrometer, without the mandatory hood. **Right**: The optomechanical design. S-B: Sample beam, shown with the Orange arrows. R-B: Reference beam, shown with the Cyan arrows. S: The integrating sphere.

The integrating-sphere equipment is operated as follows. The spectrometer is operated in double-beam mode, which compensates for lamp and detector fluctuations. In the case of reflectance (R) measurement, both 100%R and 0%R baselines are taken first. In the former, a calibrated Spectralon standard is placed on the sample port, and in the latter, the port is left uncovered. After the calibration, the reflectance of the sample will be measured relative to that of Spectralon. The true reflectance spectrum of the sample is obtained by dividing the result by the given reflectance spectrum of Spectralon.

In the case of transmission (T) measurement, the reflectance port is always covered with the Spectralon standard. The 100%T baseline is measured identically with 100%R, and the 0%T by covering the transmission port with a metal plate or otherwise nontransmitting material. After the calibration, the total transmission of a sample can be measured.

There are some caveats to the absoluteness of the R and T values measured this way. One of them is that the integrating sphere does not necessarily operate as an ideal one, and a sample that scatters differently from the standard sample will cause a different intensity distribution inside the sphere. This will lead to different internal losses and thus different response for samples that have the same true reflectance but different angular distributions of reflected radiation.

3.1 Imaging SDR setup

Other types of measurement equipment were also used in addition to the integrating sphere. For proving the concept of the next generation NIR probe, i.e. a structured illumination and spatially resolved diffuse reflectance (SDR), a camera setup was built (Figure 5 and Figure 6). The imager is the monochromatic PCO SensiCam (long-exposure model) working in the VIS spectrum. To acquire spectral images, the illumination was done using a halogen lamp and a set of 7 exchangeable narrow bandpass interference filters.

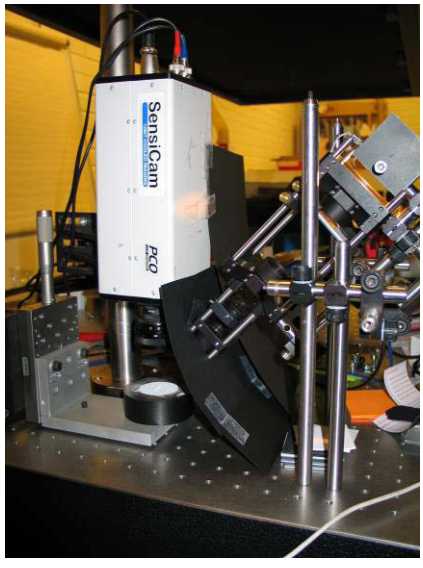

Figure 5. Lab setup for studying the structured illumination and spatially resolved diffuse reflectance, in the VIS range.

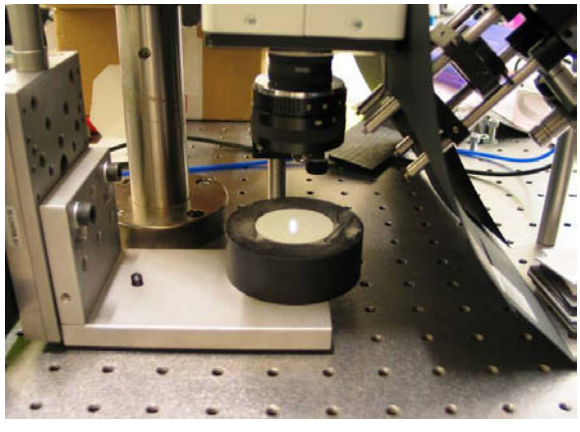

Figure 6. A detail from the lab setup. The powder is placed in the black plastic cup. The illumination strip is projected on the surface.

The operation of the SDR setup is as follows. The illumination pattern (line) is projected onto the sample surface. The pattern is brought to focus using a ground-glass sample as a reference and moving the sample lift (pictured) to the best height. The camera is also focused on the surface. The illumination intensity is adjusted using an iris shutter. A complete measurement consists of measuring

both a reference sample and a sample in the same way. The reference sample consists of a piece of 1.5 mm optical Teflon placed on top of the empty black sample cup (pictured). The bottom of the cup is furthermore covered with black velvet to minimize reflections. Thus, the reference sample approximates a 1.5 mm piece of known reference material on top of a completely absorbing layer with refractive index of 1. The optical properties of the optical Teflon have been calculated from Varian measurements.

First, one of the filters is placed in between the lamp and the condenser lens that illuminates the slit. Then the integration time of the camera is set to a value where there are no saturated pixels due to specular reflections, or only a few of them. A picture is taken, and after it the illumination is blocked and a dark picture is taken using the same integration time. This operation is repeated for each of the 7 band-pass filters. An example image of a lactose-pigment mixture is shown in Figure 7 and that of the reference sample in Figure 8.

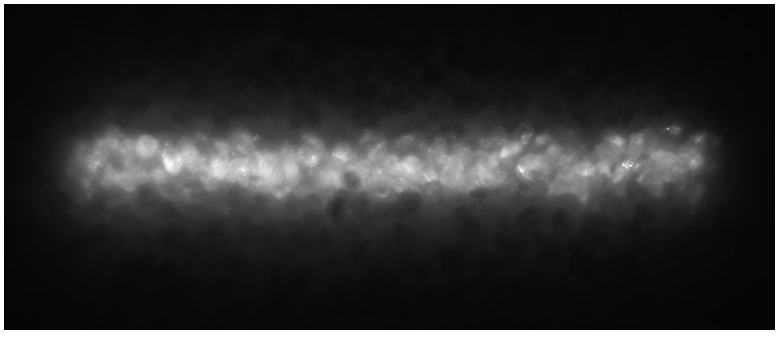

Figure 7. 50M lactose with 0.05% pigment, illuminated at 700 nm. Size of the illumination strip is 0.9 mm $\times$ 10 mm.

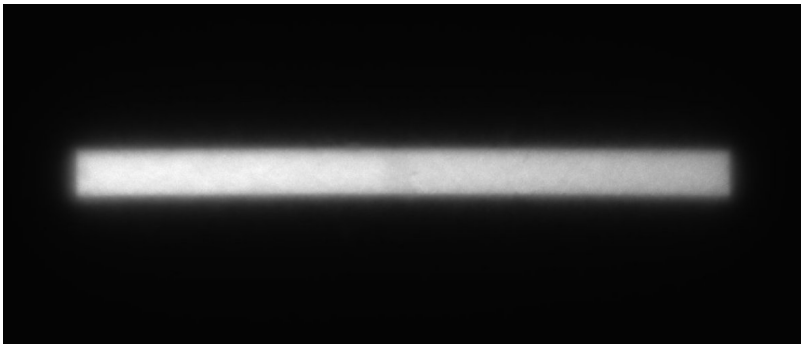

Figure 8. Spectralon standard, illuminated at 700 nm. Size of the illumination strip is 0.9 mm $\times$ 10 mm.

An example of a set of measured diffuse reflectance profiles is shown in Figure 9. In the same figure is shown the coarser five-element reflectance profile that has been used in the inversion procedure. Only five measured spectra, obtained from integrating over their respective image regions, are employed in determining the optical properties. More specifically, the inversion uses the ratios of the sample profiles to the reference profiles. In practice, because the reference material has quite large scattering coefficient and therefore a narrow reflectance profile, only the three middle spectra are usually used.

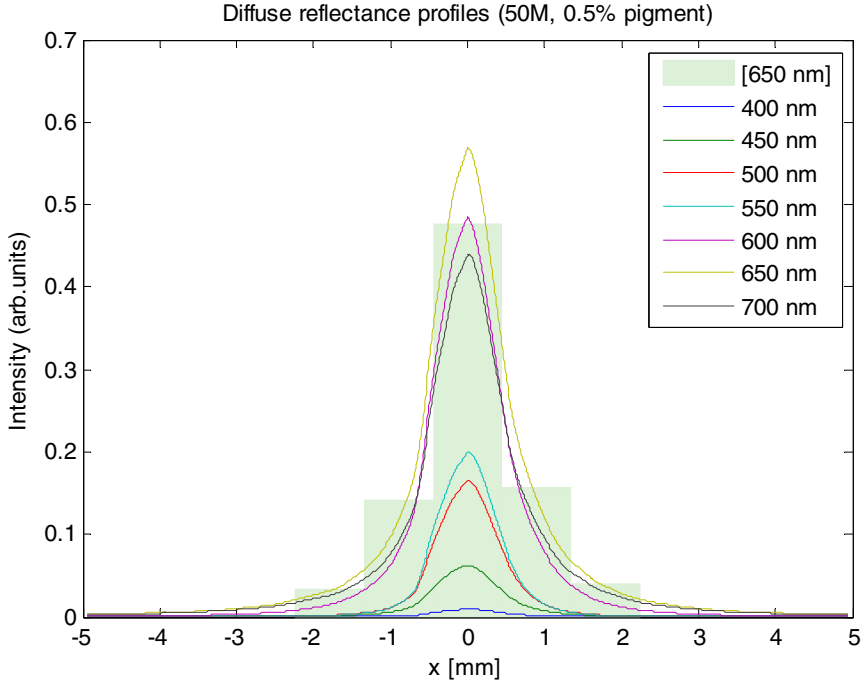

Figure 9. Measured diffuse reflectance profiles of 50M lactose with pigment.

Figure 10 shows the simulated profile spectra from the center (R0) to the right (R1 and R2). R0 is the reflectance collected from the illuminated region, R1 is the region just next to it and R2 is the region next to R1, with no direct contact to the illuminated region. Compared with Figure 1, there is certain resemblance between the diffuse transmission simulation and the R2 simulation, justifying the characterization of R2 as transmission-like measurement. The main difference between reflective and transmissive measurements is that the former increases with increasing scattering coefficient, whereas the latter decreases.

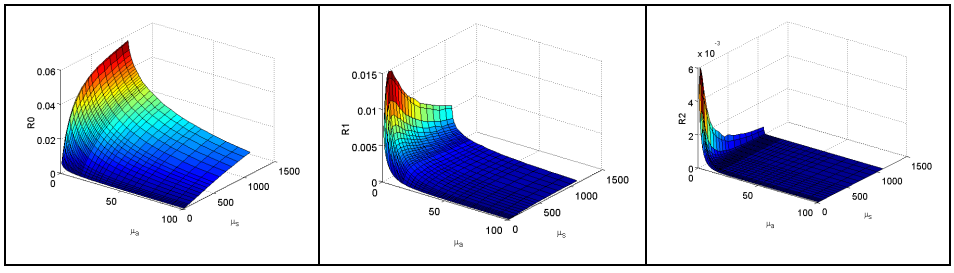

Figure 10. Simulated values of reflectances R0, R1, R2 for an optically thick sample.

4. Powder studies in VIS and NIR range

In this section the results of the integrating-sphere measurements of a range of powders are presented. The main material used was lactose monohydrate (Pharmatose by DMV International) with three mesh sizes, namely 50M, 80M and 125M (Figure 11).

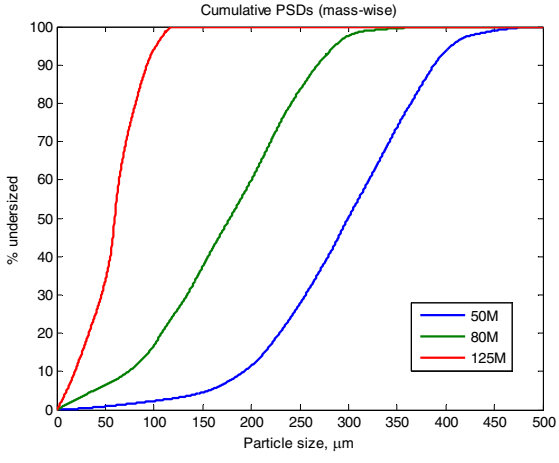

Figure 11. The cumulative particle size distributions of the lactoses.

The optical properties of pure lactoses are shown in Figure 12. One immediately sees the influence of the hidden mass effect to the absorption coefficient at wavelengths larger than 1450 nm. The apparent absorption coefficient of the finest powder (125M) is largest, for which also the small transmission in that region causes low signal-to-noise ratio. The hidden mass effect hits the 80M and 50M measurements a bit differently than one might expect. The 50M powder has the largest mean particle diameter, but still its apparent absorption coefficient is larger than that of 80M.

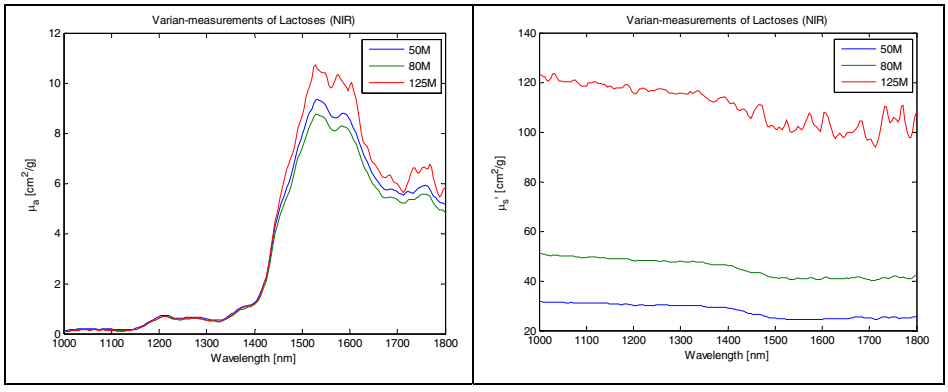

Figure 12. Optical properties of pure Pharmatoses.

4.1 Anisotropy factor of Lactose powders

The collimated transmission cannot presently be measured from the powder samples placed on top of a glass slide. For these samples, only the diffuse reflectance and transmittance can be measured using the new integrating-sphere accessory. This poses a problem, since with only two different measurement geometries, only μ_a and μ_s', but not g, can be estimated. Therefore we tried to measure the angularly resolved reflection and transmission from a "monolayer" of each of the lactoses on a quartz glass slide.

A concept image of the optical setup for these measurements is in Figure 13. The sample, which is in the middle, is illuminated using the halogen light source on top. The spectra are collected using the probes (blue-orange) which conduct the light via optical fibers to the AISA HAWK NIR spectral camera.

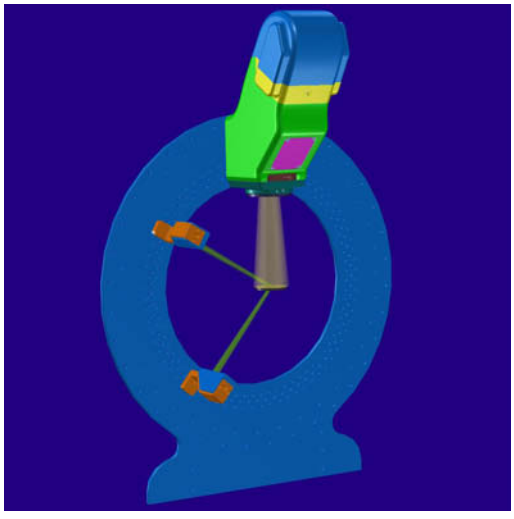

Figure 13. Mechanical design image of the device used for angularly resolved spectroscopy.

The measured angular distributions of scattered radiation at different NIR wavelengths are shown in Figure 14. For comparison, Figure 15 shows the simulated results with different trial values for g. The simulation was done in such a way that a 0.01 cm layer of material with scattering coefficient of 100 1/cm was put on top of 0.1 cm Infrasil glass slide. Absorption coefficient of the scattering layer was set to 0 and the anisotropy factor was changed. The purpose of choosing such thickness and μ_s was that on average only one scattering event would take place in the layer. Thus the simulation would correspond as closely as possible to an imaginary monolayer of particles which are now taken to be scattering centres themselves.

There is no perfect agreement between measurement and simulation at any individual wavelength or g value. However, the increasing slope of the measured spectra toward smaller scattering angles suggests a reasonably large value. We conclude that setting the anisotropy to a constant value of 0.5–0.7 should yield simulations that are accurate enough, considering all the other caveats for using RTE for powdered samples (See Section 2.1).

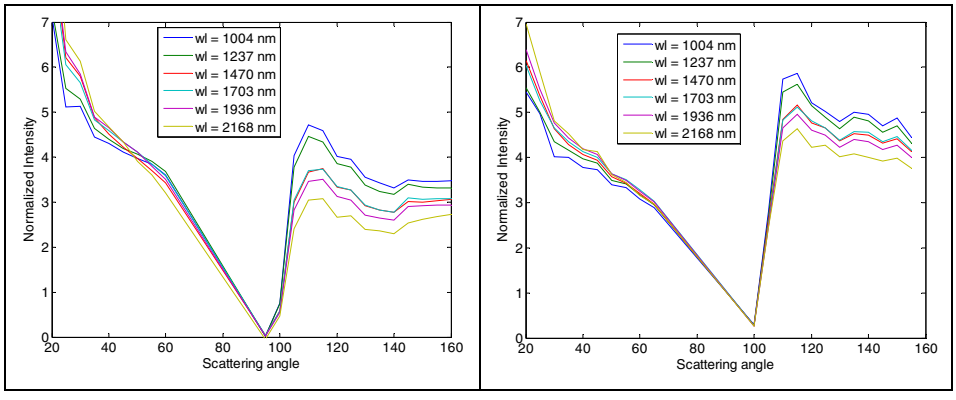

Figure 14. Measured scattered intensities of 50M (left) and 125M (right).

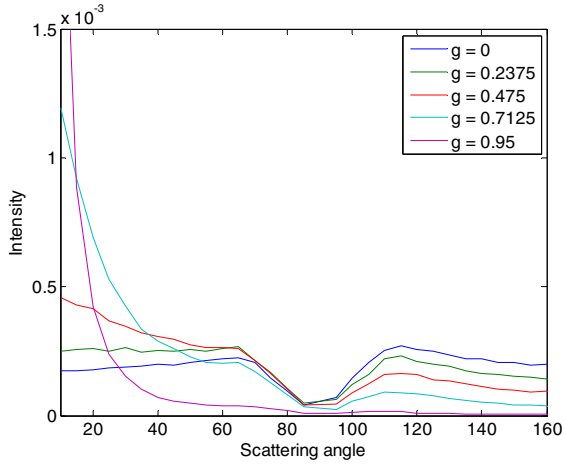

Figure 15. Simulated scattered intensities with different values of g.

4.1.1 Origin of scattering in lactose powder

There was some controversy over what causes the scattering in a lactose powder and the like. There are two possible origins. First, the surfaces that by Fresnel reflections and refractions redirect beams of light. Second, there may be microscopic scattering centres or fractures inside the particles that cause a part of the scattering. Our approach to answering the question whether it is the insides or outsides of the particles that are responsible of scattering, is as follows. We purchased a series of optical refractive-index liquids. We mixed

each liquid with as similar samples of lactose as possible in a 1 mm powder cuvette and measured the diffuse transmission of each sample in the visible wavelength region (Figure 16). The diffuse transmittances of clean 125M and 80M are 10.6% and 17.4%, respectively, so there is a substantial increase.

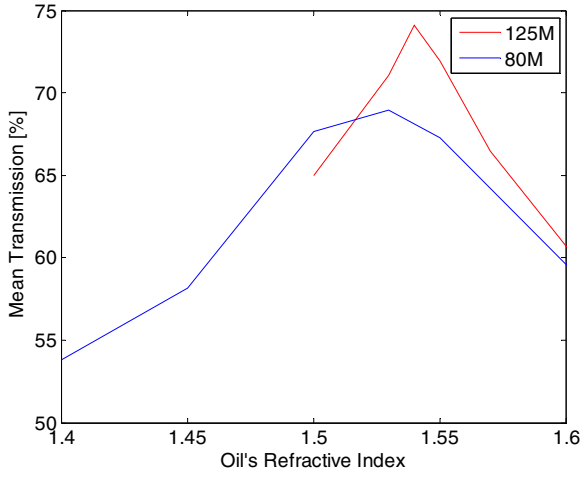

Figure 16. Mean total diffuse transmission of 1 mm oil-lactose mixtures.

At the maximum transmission the scattering is at minimum. The greatly reduced scattering is obviously visible, since one can practically read a text through the oil-lactose mixture. The transmittance of 125M increases 7-fold and that of 80M increases 4-fold. However, even the maximum transmission is nowhere near the value of 92% calculated for the non-scattering case. Thus, while with certain oil the Fresnel reflections at particle surfaces are minimized, there is still considerable residual scattering, which is stronger in 80M that has larger particle size. Now, the different dispersions of the oil and lactose may cause the transmission be minimized only in a limited wavelength region. Because the mean transmission is taken over a wide wavelength range, it includes regions where the refractive index difference and hence scattering is not minimized. In conclusion, the majority of scattering is caused by the air-lactose interfaces at particle surfaces. But the smaller transmission increase for 80M, which has larger particles than 125M, suggests that the insides of the (large) particles are not completely non-scattering either.

4.2 Lactose and Copper Sulphate mixtures

Copper sulphate ($CuSO_4$) was used as a powdered material that has some colour in the visible range unlike pure lactose. This kind of model material was needed for the imaging studies done in the VIS range (Section 4.5).

Figure 17 shows the calculated optical properties of pure lactoses and lactose-copper sulphate mixtures. To get the lactose particle size effect, both 50M and 125M lactoses were mixed with < 100µm sieved $CuSO_4$ powder fraction. It is seen that in the case of 50M, the absorption due to copper sulphate is apparently stronger than in the case of 125M. On the other hand, the absorption coefficient of lactose in the blue end of the spectrum is larger in 125M than in 50M, which is consistent with the NIR findings (Figure 12).

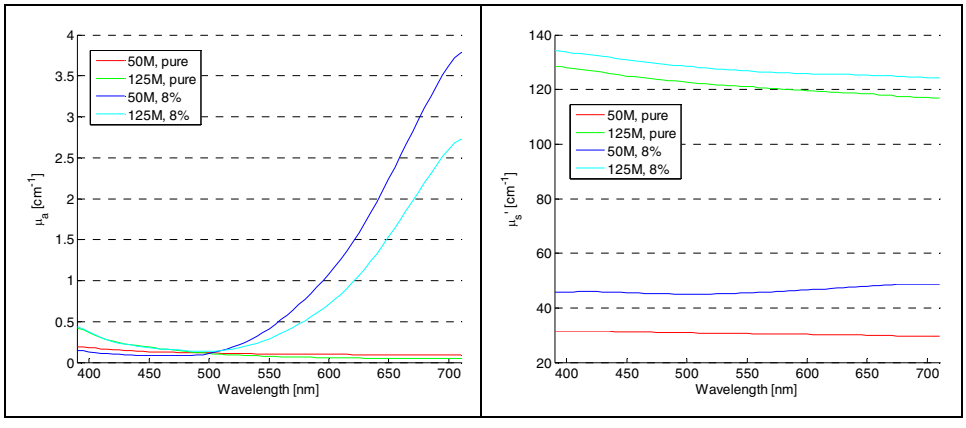

Figure 17. Absorption and scattering coefficients of lactose-copper sulphate mixtures.

4.3 Pure Copper Sulphate

Interesting tests on the effect of g on the inversion results were done using the pure Copper Sulphate powders as an example. The anisotropy factor was fixed to values 0, 0.5 and 0.7 and inversion was run, keeping other things constant. In Figure 18, we compare also the results from two different sample thicknesses of the same powder. It is seen immediately that setting g to a smaller value increases the apparent absorption coefficient and decreases the apparent isotropic scattering coefficient.

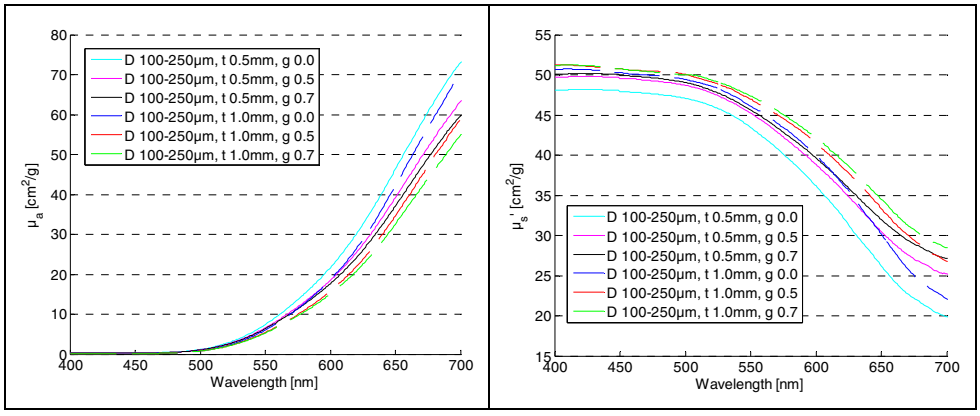

Figure 18. Diameter 100–250 µm powders (sieved), both 0.5 mm and 1 mm sample thicknesses.

4.4 Lactose and red pigment mixtures

A somewhat different material from copper sulphate, a red pigment was used as a visible model material to be mixed with lactoses. The pigment's particle size distribution extended well towards 0.1 µm in the small end. When mixed with the lactoses whose mean particle sizes are two or three decades bigger, the mixture's absorption coefficient does not behave as expected.

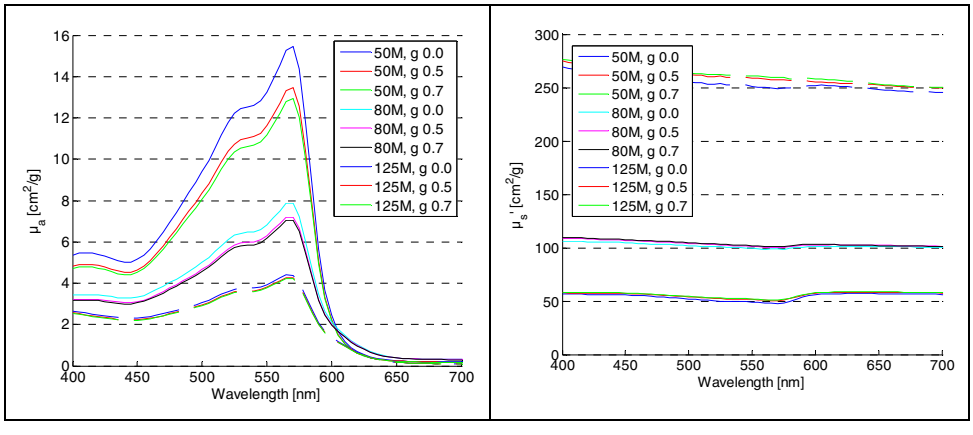

Figure 19. Lactose-pigment mixtures with 0.1% pigment.

4.5 Ascorbic acid

The optical properties of Ascorbic acid were measured. Figure 20 shows the absorption and scattering coefficient spectra of three ascorbic acid samples with different particle size distributions. Again the hidden-mass effect is seen at the 1450 nm peak. Above that the spectra are not reliable due to instrument settings.

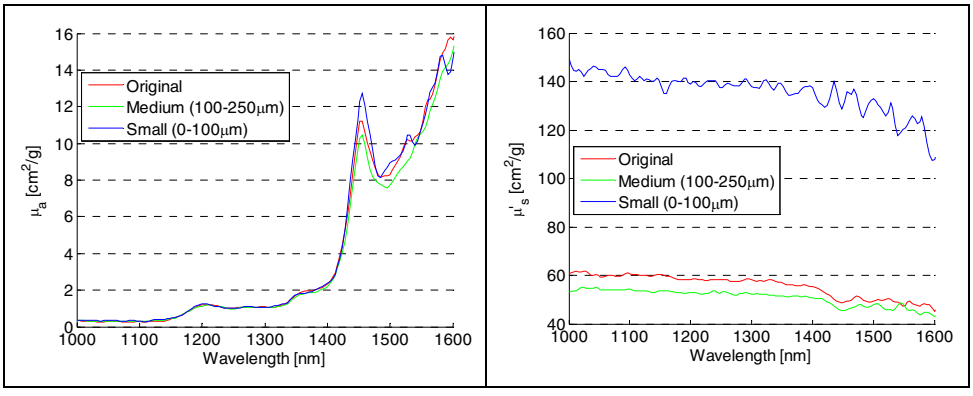

Figure 20. Optical properties of pure ascorbic acid powder. In addition to the manufacturer's default size distribution (Original), two sieved fractions were used (Medium and Small).

4.6 Spatially resolved diffuse reflectance

One of the main goals of the studies was to establish the possibility of using spatially resolved diffuse reflectance (SDR) in the "Next generation NIR probe", discussed in Section 5. This kind of feasibility study was done using the imaging setup described in Section 3. The most meaningful samples in this study were the lactose-copper sulphate and lactose/red pigment mixtures discussed in Sections 4.2 and 4.4, respectively. Also coloured-paper samples were tested, but will not be presented here.

Figure 21 shows the optical properties of two lactose-copper sulphate mixtures as measured using the imaging SDR setup. The data is to be compared with the reference values obtained with the Varian instrument. It turns out that for the finer powder, i.e. 125M, both absorption and scattering coefficient spectra match closely. With 50M the situation is much worse, a fact that is related to the large mean particle size. The effect that small CuSO particles filtrate down, while only the large lactose particles form the outermost surface, has to be taken into account also.

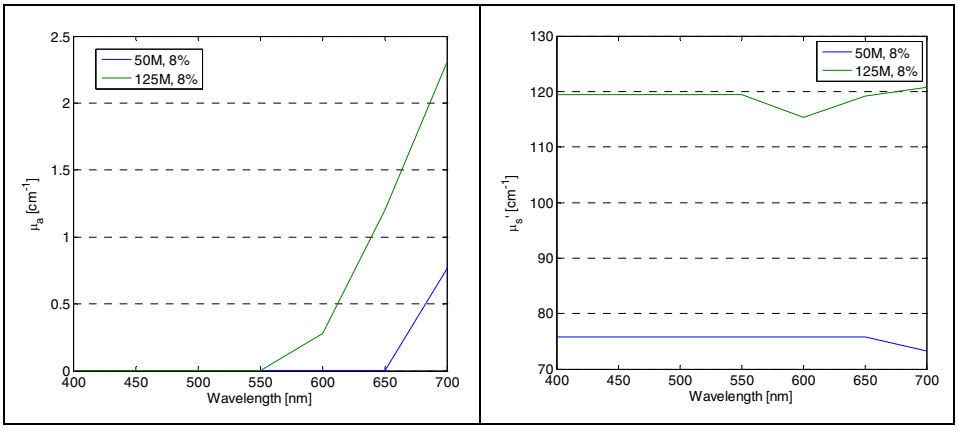

Figure 21. Optical properties of lactose-copper sulphate powder mixtures as measured using the SDR setup.

In addition to the copper sulphate powder, the red pigment was used as a visible range model API. Despite the problems found in the Varian measurements of these mixtures, the SDR measurements were carried out so as to find how well they reproduce the optical properties calculated in the former case. Figure 22 shows the comparison of inversion results for 0.1% lactose/pigment mixtures with varying lactose sizes. Figure 23 shows the results for different pigment concentrations in the case of the 50M lactose.

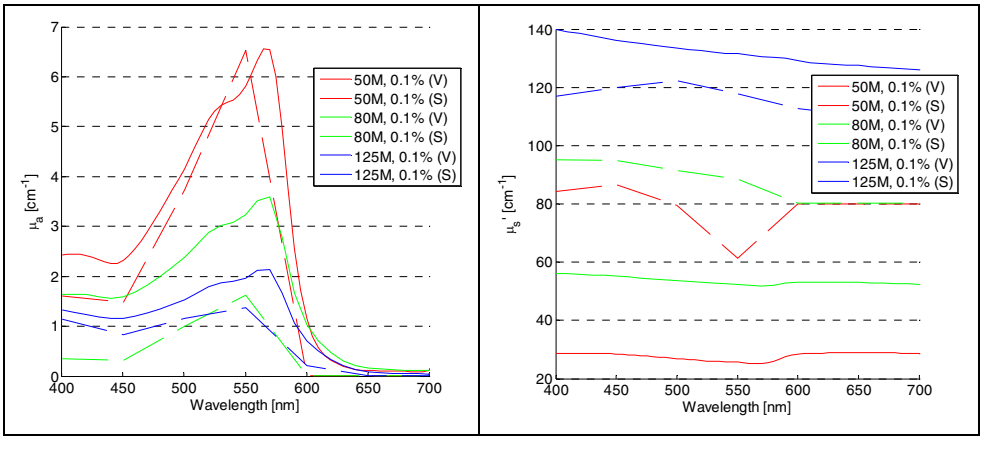

Figure 22. Optical properties of 0.1% lactose-pigment mixtures. (V): Varian measurements, (S): SDR measurements.

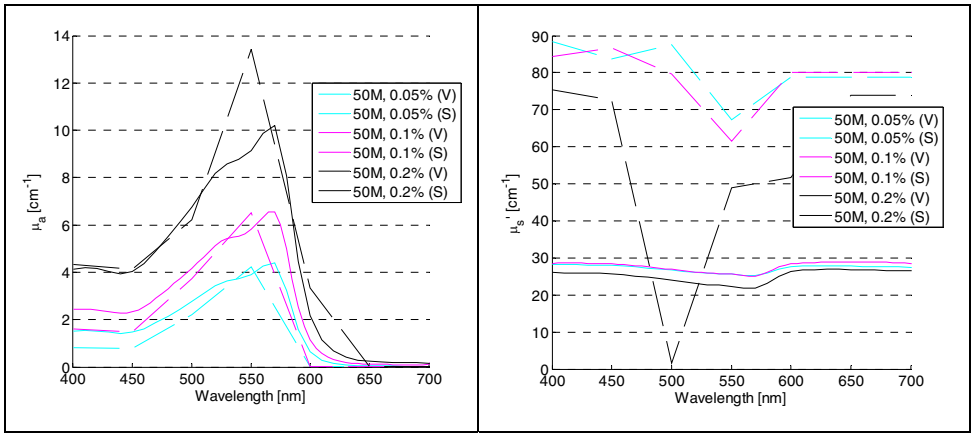

Figure 23. Optical properties of mixtures of 50M lactose and red pigment. (V): Varian measurements, (S): SDR measurements.

5. Next generation NIR probe

The original assignment of the WP 1.1 was to build a wireless on-line mixing homogeneity probe for pharmaceutical powder mixers. This goal could not be met, for reasons that will be discussed below. First we will describe some of the principles behind the blend homogeneity measurement, then the “next generation NIR” approach, and last the problems that were encountered.

The requirement is to be able to measure the concentration of the API in the excipient. The interrogated sample size must correspond approximately to the amount of powder making one tablet. We will call this the unit sample. The measurement must be done through a window embedded in the wall of the mixer. Blending can be, and is, often assessed using single-point NIR diffuse reflectance measurement. The simplest approach that applies to batch processes is to measure a time series of spectra during mixing and observe the instant when a static condition is attained. In this phase it is known that, since the spectra of different samples of the batch are the same, the concentration must be homogeneous and determined by the ratios of the input materials. There probably will not be a completely static phase however. If there are physical changes to the materials due to beating or agglomeration that develop through time, the NIR spectra will exhibit time trends even if mixing homogeneity were already reached. Also, depending on the size of the unit sample, occurrences of partial demixing are more or less common and will cause some noise in the static phase.

The problem of mixing is to know whether each randomly picked unit sample in a batch has the same mass of the active pharmaceutical ingredient. In practice, because the concentration cannot be exactly the same, the question is whether the variance between unit samples is in given acceptable limits. The physical size and shape of the particles can be allowed to vary in certain given limits from unit sample to unit sample. In general, both the amount of API and the physical

form of the API and excipient particles are of interest since the latter affects e.g. the solubility of the drug in the body. In principle both the chemistry and the physics can be inferred from a reflectance spectrum, since the scattering differences due to particle size changes have a certain signature effect on the spectra. But it is hard to make these measurements reliable due to the need of extensive calibration sample sets.

On the other hand, in the “next generation” approach the measurement consists of at least two simultaneous spectra measured from the same approximate location but in both transmission- and reflection modes. The transmission mode is understood here in the sense used in spatially resolved diffuse reflectance spectroscopy. It is simply the diffuse reflectance measured at some distance from an illumination spot, and unlike the transmission measurement in the familiar sense it requires the presence of scattering. The reflection mode on the other hand is measured from within the illuminated region. In a sense the two-mode measurement provides the user with two times more information per wavelength than reflectance measurement alone. This is because the transmission mode sees only photons that have travelled certain minimum path length inside the sample, whereas the reflection mode sees a wide range of path lengths starting from zero. Thus changes in the absorption- and scattering properties of the sample material have different and to some degree independent effects on the two spectra. It is roughly the case that for each wavelength there is a one-to-one correspondence between the set two measurements and the two optical properties, namely absorption and scattering coefficients. The absorption coefficient measured at an absorption band of the API changes linearly with the concentration, whereas physical changes like that of the particle size are embedded in the scattering coefficient. The problems associated with this notion are touched also in the section 2.1 on light propagation models.

When it works, the next-generation approach provides concentration measurement independent of physical changes of the mixture. Therefore it would be applicable not only to batch mixing processes but for continuous processes also, like continuous granulation.

The problem is that the assumption does not hold that it is possible to neatly separate the scattering and absorption properties of all samples. The assumption would be that changing the particle size of a pure powdered substance would only affect the measured scattering coefficient, but in reality it will change the apparent absorption coefficient also. This basically invalidates the idea of the particle size-independent concentration measurement. It was found that unless a

better way of modelling the light propagation in particle mixtures is devised, there are severe limitations to the use of the “next generation” principle.

All in all, the reasons of deciding not to build the original on-line prototype were the observed limitations of its physical working principles. Therefore the course of action was steered towards a laboratory instrument with appreciable flexibility for experimentation. The principle of operation is to combine structured illumination with spatially resolved diffuse reflectance measurement. The illuminated area is chosen approximately to measure a unit sample at a time.

5.1 Design of the lab instrument

Structured illumination means *in this case* that a pattern of illuminated and un-illuminated regions is created on the sample surface. This is attained by illuminating one side of a metal mask with the desired pattern of holes and projecting the image of the other side on the sample. The mask containing the illumination pattern will be hence called *illumination mask*.

The spatially resolved diffuse reflectance measurement in the instrument is done using any suitable spectrometer with optical fiber connection. Just as with the illumination mask but in the reverse direction, the end of the collection fiber is projected, with appropriate scaling, on one side of another metal mask with appropriate hole-pattern. The image of the other side of the mask in turn is projected on the sample, on top of the illumination pattern. The mask bearing the collection- or pick-up pattern will be hence called *pick-up mask*.

One easy way to understand the meaning of the pick-up mask is to imagine that instead of a spectrometer, the optical fiber is coupled to a light source. Then, tracing backwards, the fiber illuminates the pickup mask and the pattern is imaged on the sample. The regions that are thus lit up would be the regions where diffusely reflected light is otherwise collected.

Let the sample surface be located in (x, y) plane and the positive z-axis extend inside the sample. Let P_c denote the union of those regions of the 2-dimensional pick-up pattern that are picked up in a measurement. Thus P_c consists of the lit regions of the thought experiment in the previous paragraph. At each point belonging to P_c, the pick-up optics collect the portion of radiant exitance that fits inside the optics’ numerical aperture, or in other words the acceptance cone. The power collected in the optical fiber is therefore proportional to

$$W_c = \iint_{P_c} \left[\iint_{\Delta\Omega_c} L(x,y;\theta,\phi) \cos\theta \mathrm{d}^2\Omega \right] \mathrm{d}x\mathrm{d}y \,, \tag{5-1}$$

where L is radiance, $\Delta\Omega_c$ denotes the spatial angle making up the acceptance cone and (θ,ϕ) the polar and azimuthal angles. Similarly, the power incident on the sample with given illumination pattern P_i is written as

$$W_i = \iint_{P_i} \left[\iint_{\Delta\Omega_i} L(x,y;\theta,\phi) \cos\theta \mathrm{d}^2\Omega \right] \mathrm{d}x\mathrm{d}y \,, \tag{5-2}$$

where $\Delta\Omega_i$ denotes the spatial angle inside the numerical aperture of the illumination.

Illumination mask is kept stationary so that the illumination pattern on the sample does not move. The pick-up mask on the other hand is made movable. Therefore the pick-up pattern P_c can be moved to different locations over the illumination pattern. This is to collect diffuse reflection from both directly illuminated regions and those where also or only diffused light is available.

The design of the prototype instrument is shown in Figure 24. Both illumination and pick-up sides use Offner optics to image the mask surfaces onto the sample surface. The Offner optics has two major advantages. First, being based on mirrors only, there is no chromatic aberration which would become a serious problem since the wavelength range of the instrument is specified to be 400–2500nm. Second, the magnification (1x) stays constant over the whole field of the obliquely imaged masks. On the illumination side, a mixer tube made of polished and coated aluminium ensures uniform illumination of the mask, keeping also the angles of incidence compatible with the acceptance cone of the imaging optics over the whole mask area. On the pickup side, Köhler optics is employed to collect the light evenly from the relevant mask region and guide it to the fiber. Two motorized linear stages move the packet containing the mask, the optics and the fiber connector.

The basic operational principles of the measurement setup are depicted in Figure 25. A computer controls both the movement of the pickup mask and the timing of the spectroscope that acquires the spectra at given pickup pattern locations. The lamp receives its power from an external power source with voltage stabilization.

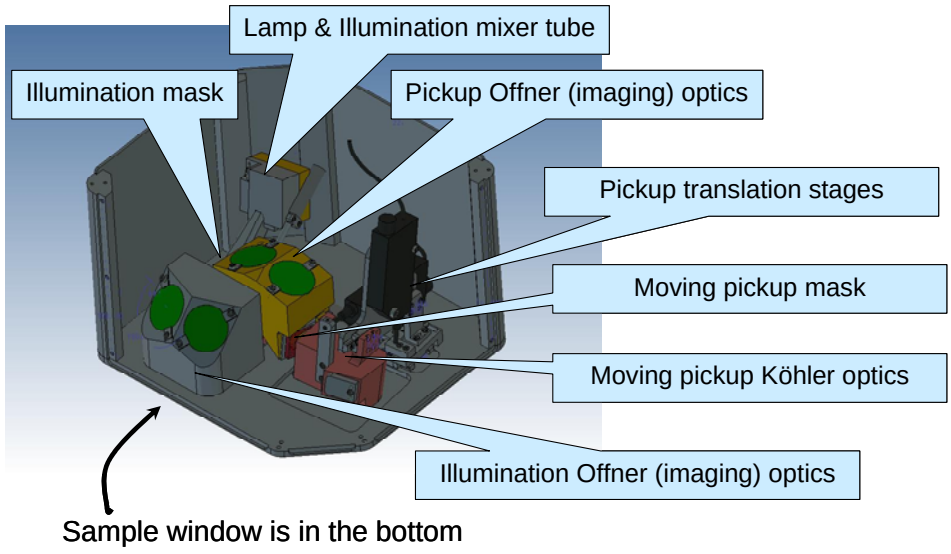

Figure 24. Optomechanical design picture of the prototype. Part of the cover has been removed.

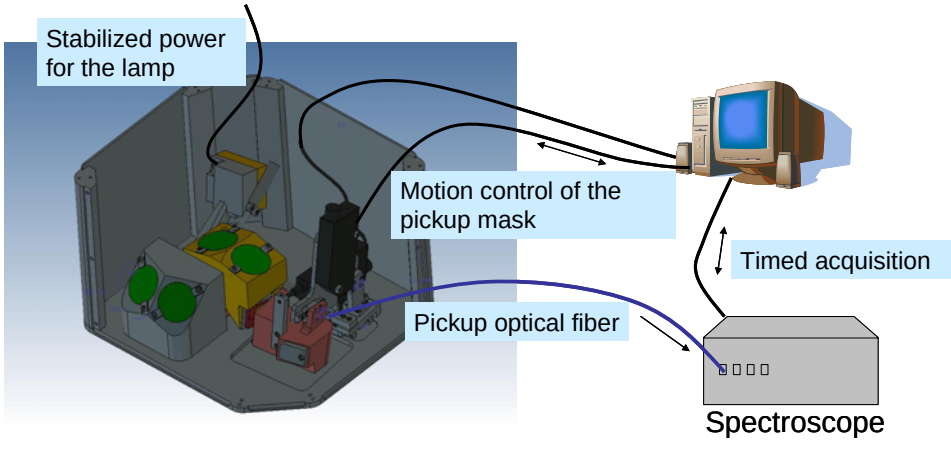

Figure 25. Operation principles of the prototype.

The optomechanical assembly of the illumination optics is depicted in Figure 26. The light source (LS) projects the image of the fiber to the narrow end of the mixer tube (MT) that spreads the light evenly on the illumination mask (IM). The imaging Offner optics consists of the three spherical mirrors (SM1, SM2, SM3). The light path from the mask to the Offner optics is folded using the

planar mirror (PM) to move the light source away from the sample space. To compensate for the astigmatism and chromatic aberration caused by the sample window (W), three equally thick compensators (C1, C2, C3) have been added to the light path. The focus adjustment stage (FA) moves the mask, the mixer tube and the light source along the optical axis.

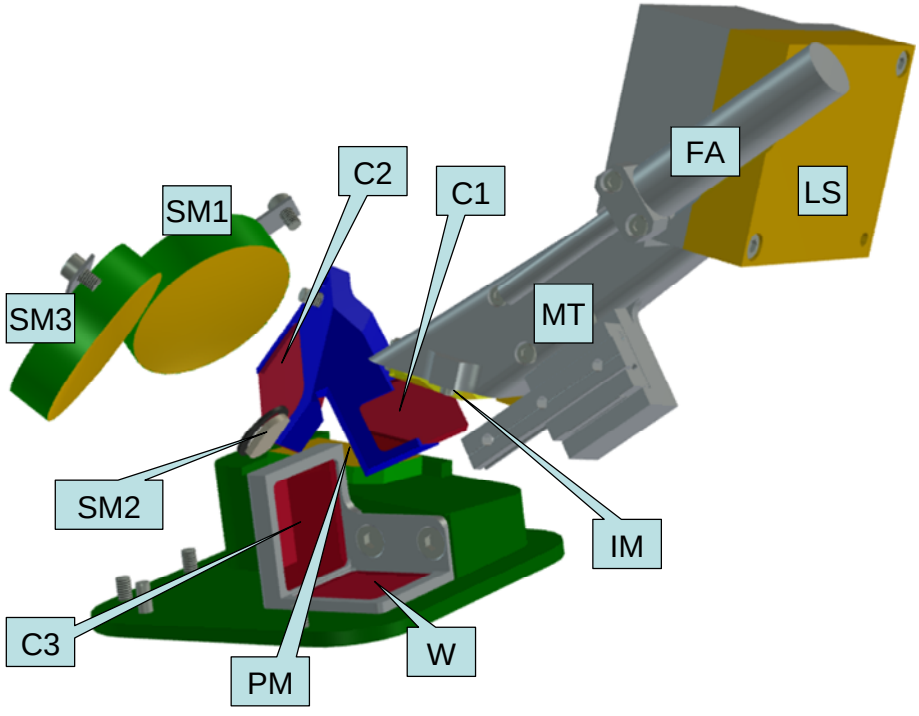

Figure 26. Optomechanical components of the illumination side of the prototype.

The optomechanical setup of the pickup side in the prototype design are shown in Figure 27. The Offner optics that image the sample region onto the pickup mask comprise of the spherical mirrors SM1, SM2, SM3 that are identical to those in the illumination side. The light path begins from the bottom surface of the sample window (W), continues through SM1, SM2 and SM3, after which the beam is folded to the side using a planar mirror (PM1). Before arriving at the mask surface (CM), the beam passes through the compensator window C. After the mask, the light originating at all points of the mask's rear surface must be guided with equal efficiency to the fiber connector FC. This is achieved by the len ML1 in contact with the mask, the planar mirror PM2 and the two elliptical

mirrors EM1 and EM2. The optics between the mask and the fiber connector are best understood if one thinks the situation in reverse, i.e. that the fiber is used for illumination. In this case, the elliptical mirrors basically produce a Köhler illumination on the mask surface, after the beam has been folded with the mirror PM2. The lens refracts the beam cones at each point of the mask in the appropriate direction for the Offner optics to pick up. In other words, the lens helps fill the numerical aperture of the Offner optics equally in all field points. The Offner optics then simply images the illuminated “pickup pattern” on the sample located below the window W.

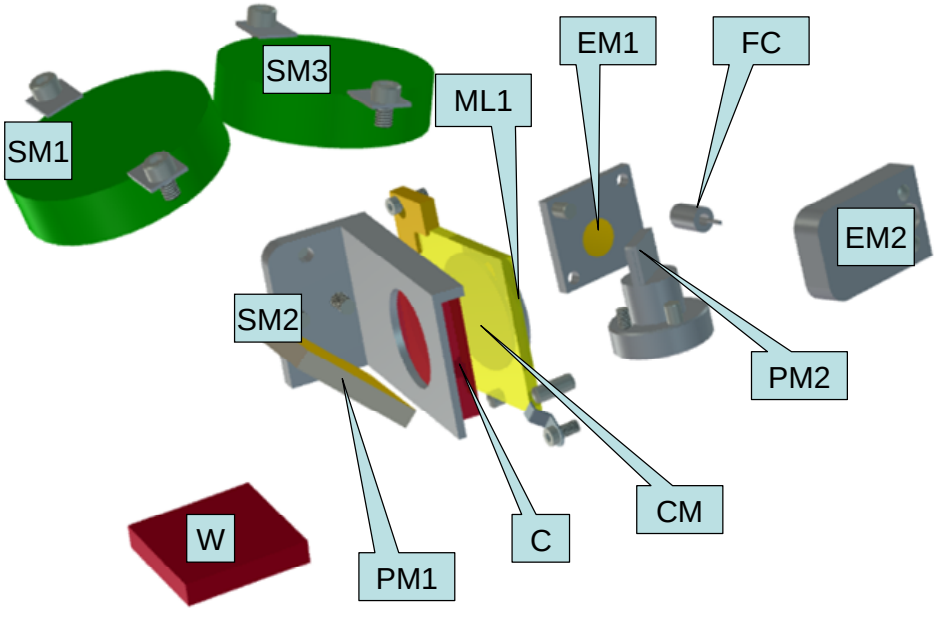

Figure 27. Optomechanical components of the pickup side of the prototype.

The next-generation NIR laboratory probe is yet to be manufactured. The design is very complicated, including several complicated and expensive parts that have to be assembled to high tolerances. From the user perspective, the routine modifications of the device are not simple or fast. For example changing the illumination or pick-up pattern is necessarily cumbersome. Removal and replacement of the window and accompanied compensator plates is also difficult. There is also no easy way of focusing the illumination and pickup patterns in NIR wavelength region, although it is possible in the visible region.

5.2 Potential online instrument designs

The laboratory prototype described above is not well suited to heavy industrial use due to its delicate mechanics. Also the optical design with masks is not optimized for efficient use of radiometric power available from the lamp. The majority of the flux is typically lost in the opaque regions of the masks. Therefore the integration times will be long especially for strongly absorbing samples. This is acceptable in the lab prototype, because the main design concern was the flexibility to choose illumination and pickup patterns.

A more power-optimized SDR probe consists of a properly arranged fiber bundle with fibers dedicated both to illumination and pickup. The end of the bundle is imaged, with a chosen magnification, onto the sample surface. Stronger scatterers and absorbers would require smaller magnification and weaker scatterers a larger magnification to obtain the necessary separations of the order of $1/\mu'_t$ between illumination and pickup spots. One downside of this kind of arrangement is that when in focus, a pickup spot cannot overlap an illumination spot. To achieve some overlap, the image on the sample must be brought out of focus.

5.2.1 Mask manufacturing

The illumination- and pickup masks are two critical components of the system. Two methods for their manufacturing were tried in Laserprobe inc., Oulu. The first method is to laser-cut the features (stripes etc.) to a thin sheet of a special metal alloy. These kind of masks were employed in the lab SDR setup described above.

However, in the case of large (about 1 cm^2) strip patterns, there is the risk of spontaneous deformation from plane. This would cause distortions in the illumination pattern. Therefore a second method was developed. A thin layer of metal was sputtered on top of quartz glass, and the mask features were lasered to that layer. It was found that a 200–300 nm layer of Tungsten was very good in terms of feature quality and transmission in the regions meant to be opaque. These masks have the good property of staying planar even when heated. Their downside is the scattering at the glass surface where the metal has been vaporized. This scattering, along with some residual transmission through the metal, decreases contrast compared to the first type of masks.

5.3 Other measurement approaches

The problem of determining API concentration in an excipient from a surface measurement calls for an imaging approach. Hyperspectral imaging in the NIR range provides in principle a straightforward way of *counting* API particles. When the image is taken at a wavelength belonging to a suitable absorption band of the API material, the particles are seen as dark spots in the background consisting of the excipient. Evaluating the combined area of the dark spots divided by the total area of the image gives an easy estimate of the concentration.

However, the same problem as with the traditional reflectance spectroscopy, namely diffusion, comes into play in the imaging approach. The particle layer of powder mixture nearest the window is not the only one that contributes to the measurement, but layers beneath the surface easily distort the signal.

Depending on the size differences and absorption coefficient differences of the API and excipient, it might be difficult to find a wavelength where the image contrast would be sufficient. Also, the case of extremely small API particles requires both expensive optics and large-resolution imaging cells (CCD).

A hyperspectral imaging system combined with one type or another of structured illumination would provide a means of both calculating API particles and estimating diffusion. The diffusion is of course dictated by the scattering- and absoption properties of the powder mixture. There is already commercial image analysis software for calculating particle size- and shape distributions using normal 2D images. Using optical wavelengths, it is very difficult to obtain a 3D surface profile of transparent particles from a reflectance image. Therefore the structured illumination and hyperspectral imaging separate out all practically available effects that are seen, but concealed, in traditional NIR reflectance spectroscopy.

The *coherent backscattering* phenomenon could be used to obtain depth-resolved information about a scattering and absorbing sample.

6. Conclusions

An integrating-sphere accessory for diffuse reflectance and transmittance measurements of powder samples was designed and built. The accessory makes it possible to measure horizontally positioned samples. It was designed to be used with the Varian Cary 5000 spectrophotometer.

Also a camera-based system, for measuring the spatially resolved diffuse reflectance (SDR) in the VIS range, was built.

The scattering- and absorption properties of several different powders and powder mixtures were measured using the integrating-sphere accessory. The results were compared in the visible range with the SDR results. It was found that the results agree to a reasonable degree, taking into account all experimental errors including the nature of the samples.

However, while there is an agreement between methods, the agreement also confirms the failure of the radiative transfer model as a predictor of concentrations in coarse powders. Not only the hidden-mass effect but other effects, present in mixtures, make it so.

The wireless blend homogeneity sensor prototype that was planned for the WP 1.1 could not be realized. The reason for this was that the measurement principle originally proposed was found to be unsound, as mentioned above. It was found that diffuse reflectance from powder samples of moderately large sizes, does not generally follow the predictions of the radiative transfer model. From this it follows that optical measurement of API concentrations in pharmaceutical mixtures based on first-principles models does not currently work.

After this finding, it was decided that instead of building a prototype for inline testing, a laboratory research device would be designed and built. The purpose of this device would be to extensively test the principle of structured illumination with spatially resolved diffuse reflectance, with a variable set of samples. To be useful, the device had to be versatile in terms of wavelength,

illumination patterns and the types of sample that could be measured. These requirements led to the situation that the instrument's optomechanical design became excessively complicated and prone to errors.

Also the finishing of the design and manufacturing of the laboratory device had to be suspended, because the budget for WP1.1 was exceeded due to the inclusion of the multipoint NIR instrumentation to it. After re-evaluation of the benefits and risks of the current design concept, it was decided that we will not pursue it further, but rather choose the imaging or other alternative (described above) in future projects.

The main achievements of the work package were the development of laboratory equipment and a flexible software package to measure the optical properties of reasonably homogeneous materials.

References

Bohren, C.F. & Huffman, D.R. 1998. Absorption and Scattering of Light by Small Particles. 1st ed. USA: John Wiley & Sons, Inc.

Burger, T. & Fricke, J. 1998. NIR radiative transfer investigations to characterise pharmaceutical powders and their mixtures. Journal of Near Infrared Spectroscopy, Vol. 6, pp. 33–40.

Burger, T., Kuhn, J., Caps, R. & Fricke, J. 1997. Quantitative Determination of the Scattering and Absorption Coefficients from Diffuse Reflectance and Transmittance Measurements: Application to Pharmaceutical Powders. Applied Spectroscopy, Vol. 51, No. 3, pp. 309–317.

Chandrasekhar, S. 1960. Radiative transfer. Dover.

Dahm, D.J. & Dahm, K.D. 2007. Interpreting Diffuse Reflectance and Transmittance. Chichester, UK: IM Publications.

Fantini, S. & Franceschini, M.A. 2002. Frequency-Domain Techniques for Tissue Spectroscopy and Imaging. In: Anonymous Handbook of Optical Biomedical Diagnostics. Vol. 1. Washington, USA: SPIE. Pp. 405.

Green, K., Lamberg, L. & Lumme, K. 2000. Stochastic modeling of paper structure and Monte Carlo simulation of light scattering. Applied Optics, 1 September 2000, Vol. 39, No. 25, pp. 4669–4683.

Jacques, S.L. & Pogue, B.W. 2008. Tutorial on diffuse light transport. Journal of Biomedical Optics, July/August 2008, Vol. 13, No. 4, pp. 041302.

Kim, A.D., Jaruwatanadilok, S., Ishimaru, A. & Kuga, Y. 2001. Polarized light propagation and scattering in random media. Proceedings of the International Society for Optical Engineering (SPIE) 4257. Pp. 90–100.

Maheu, B., Letoulouzan, J.N. & Gouesbet, G. 1984. Four-flux models to solve the scattering transfer equation in terms of Lorenz-Mie parameters. Appl. Opt., Vol. 23, No. 19, pp. 3353–3362.

Mandelis, A., Boroumand, F. & van den Bergh, H. 1990. Quantitative diffuse reflectance spectroscopy of large powders: the Melamed model revisited. Applied Optics, 1 July 1990, Vol. 29, No. 19, pp. 2853–2860.

Metropolis, N. & Ulam, S. 1949. The Monte Carlo Method. Journal of the American Statistical Association, September 1949, Vol. 44, No. 247, pp. 335–341.

Mishchenko, M.I., Travis, L.D. & Lacis, A.L. 2002. Scattering, Absorption, and Emission of Light by Small Particles. Cambridge.

Rozé, C., Girasole, T. & Tafforin, A. 2001. Multilayer four-flux model of scattering, emitting and absorbing media. Atmospheric Environment, Vol. 35, pp. 5125–5130.

Wang, L., Jacques, S.L. & Zheng, L. 1995. Monte Carlo modeling of light transport in multi-layered tissues. Computer Methods and Programs in Biomedicine, Vol. 47, pp. 131–146.

Wendlandt, W.W. & Hecht, H.G. 1966. Reflectance Spectroscopy (Chemical Analysis). First ed. John Wiley & Sons Inc. 306 p.

Yaroslavsky, I.V., Yaroslavsky, A.N., Goldbach, T. & Schwarzmaier, H. 1996. Inverse hybrid technique for determining the optical properties of turbid media from integrating-sphere measurements. Applied Optics, Vol. 35, No. 34, pp. 6797–6809.

Series title, number and report code of publication

VTT Publications 703
VTT-PUBS-703

Author(s)
Lauri Kurki & Ralf Marbach

Title

Radiative transfer studies and Next-Generation NIR probe prototype

Abstract

As a part of the PAT-KIVA project, this report summarizes the results of the work packages (WP's) 1.1 and 1.4. The WP1.4 consisted of laboratory studies to measure the absorption and scattering properties of several pharmaceutical powders. It also included the designing and building of the spectrometer accessories to make the measurements possible. The WP1.4 was needed to support of the WP1.1, where a wireless online probe of powder blend homogeneity was to be built. The idea was to be able to separate the chemical concentrations from the physical determinants of the powder blends by spatially resolved diffuse reflectance spectroscopy (SDR). The chemical concentrations were assumed, according to previous studies by others, to be faithfully represented in the calculated absorption coefficient. On the other hand, the physical properties like particle size distribution were assumed to be separated into the scattering coefficient and anisotropy factor. However, the studies indicated, that with the growth of particle size, these assumptions do not hold to any reasonable degree. Therefore it was decided not to design the online probe, but a laboratory research probe employing the SDR principle and being as versatile as possible regarding the wavelength range and illumination features. The design of the laboratory probe was nearly completed, but due to various reasons, it could not be built within the PAT-KIVA project. The main results of the WP1.4 were the building of spectrometer accessories and the measured optical properties of various powders. The main results of the WP1.1 were the preliminary comparison of SDR measurements to the "reference" measurements done in WP1.4, and the near completion of the very challenging design task of the laboratory SDR probe. Another main result connected with both work packages was the development of simulation software to solve the inverse problem of calculating samples' optical properties from spectroscopic measurements.

ISBN
978-951-38-7137-6 (soft back ed.)
978-951-38-7333-2 (URL: http://www.vtt.fi/publications/index.jsp)

Series title and ISSN	Project number
VTT Publications 1235-0621 (soft back ed.) 1455-0849 (URL: http://www.vtt.fi/publications/index.jsp)	

Date	Language	Pages
January 2009	English	43 p.

Name of project	Commissioned by
PAT-KIVA	

Keywords	Publisher
NIR, spectroscopy, Monte Carlo, radiative transfer, diffusion, SDR, diffuse reflectance, diffuse transmittance, structured illumination	VTT Technical Research Centre of Finland P.O. Box 1000, FI-02044 VTT, Finland Phone internat. +358 20 722 4520 Fax +358 20 722 4374

VTT PUBLICATIONS

688 Mervi Hirvonen. Performance enhancement of small antennas and applications in RFID. 2008. 45 p. + app. 57 p.

689 Harri Setälä. Regio- and stereoselectivity of oxidative coupling reactions of phenols. Spirodienones as construction units in lignin. 2008. 104 p. + app. 38 p.

690 Florian Mirianon, Stefania Fortino & Tomi Toratti. A method to model wood by using ABAQUS finite element software. Part 2. Application to dowel type connections. 2008. 55 p. + app. 3 p.

691 Tomi Räty. Architectural Improvements for Mobile Ubiquitous Surveillance Systems. 2008. 106 p. + app. 55 p.

692 Kimmo Keränen. Photonic module integration based on silicon, ceramic and plastic technologies. 2008. 101 p. + app. 70 p.

693 Emilia Selinheimo. Tyrosinase and laccase as novel crosslinking tools for food biopolymers. 2008. 114 p. + app. 62 p.

694 Olli-Pekka Puolitaival. Adapting model-based testing to agile context. 2008. 69 p. + app. 6 p.

695 Minna Pikkarainen. Towards a Framework for Improving Software Development Process Mediated with CMMI Goals and Agile Practices. 2008. 119 p. + app. 193 p.

696 Suvi T. Häkkinen. A functional genomics approach to the study of alkaloid biosynthesis and metabolism in Nicotiana tabacum and Hyoscyamus muticus cell cultures. 2008. 90 p. + app. 49 p.

697 Riitta Partanen. Mobility and oxidative stability in plasticised food matrices. The role of water. 2008. 92 p. + app. 43 p.

698 Mikko Karppinen. High bit-rate optical interconnects on printed wiring board. Micro-optics and hybrid integration. 2008. 162 p.

699 Frej Wasastjerna. Using MCNP for fusion neutronics. 2008. 68 p. + app. 136 p.

700 Teemu Reiman, Elina Pietikäinen & Pia Oedewald. Turvallisuuskulttuuri. Teoria ja arviointi. 2008. 106 s.

701 Pekka Pursula. Analysis and Design of UHF and Millimetre Wave Radio Frequency Identification. 2008. 82 p. + app. 51 p.

703 Lauri Kurki & Ralf Marbach. Radiative transfer studies and Next-Generation NIR probe prototype. 2009. 43 p.

ISBN 978-951-38-7137-6 (soft back ed.)
ISSN 1235-0621 (soft back ed.)

ISBN 978-951-38-7133-2 (URL: http://www.vtt.fi/publications/index.jsp)
ISSN 1455-0849 (URL: http://www.vtt.fi/publications/index.jsp)